Commentationes Physico-Mathematicae

Vol. 42 No. 2
June 1972

A Method for Transversal Tomography using Gamma Radiation, Transversal Transmission Gammatomography, AHTI REKONEN

Societas Scientiarum Fennica
Helsinki - Helsingfors

Verkkoversio julkaistu tekijän ja
Suomen Tiedeseuran luvalla.

URN:ISBN:978-951-39-9994-0
ISBN 978-951-39-9994-0 (PDF)

Jyväskylän yliopisto, 2024

Keskuskirjapaino—Centraltryckeriet
Helsinki 1972 Helsingfors

Commentationes Physico-Mathematicae
Vol. 42 1972

A method for transversal tomography using gamma radiation. Transversal transmission gammatomography

Ahti Rekonen
Middle Finland Central Hospital and
Department of Physics, University of Jyväskylä
Jyväskylä, Finland

Abstract: The present work introduces a new transversal tomography procedure, where the radiation source is a gamma-rays emitting radionuclide and the detector a scintillation counter. The procedure involves transversal and rotary motion of the collimated gamma-ray beam at the emitter-detector unit relative to the subject. The modulation transfer functions are calculated for each component unit, for the motions and finally for the complete system. A comparison indicates that the developed *transversal transmission gammatomography* (TTGT) ranks in terms of image resolution above radioisotope scintigraphy though lower than roentgen transversal tomography. The radiation load in the TTGT process is clearly smaller than that of conventional X-ray or scintigraphic methods. Some results and photographs of phantom and patient tomograms are presented.

1. Introduction

The use of transmitted radiation to obtain an image representation of the internals of a subject is continuously increasing. The last two decades have seen radionuclides grow in importance as a means of acquiring this pictorial information in addition to the known methods of roentgen radiography. The application of both roentgen and gamma radiations have resulted in the development of many specialized procedures which are rather similar in the way in which the image is formed.

One class of application is sectional radiography, i.e. linear and transversal tomography. Tomographic processes employing X-rays already form part of the classical repertory. On the other hand, the use of radionuclides is still in its infancy; for instance, the first common linear tomograph using isotopes, developed by Muehllehner[1], became commercially available as recently as in 1971.

Transversal tomography, which gives the pictorial representation of a cross-section of a subject, is mostly used in radiotherapy, especially in

treatment planning. To select the optimal direction of the radiation field and to apply the proper dosimetric correction factors required by the density differences of the tissues, the transversal position of the various organs, the differences in these densities and their cross-sectional outlines must be known.

A tomogram of a transversal plane can be made through one of three basic methods:

- methods which use the differences in the densities of the various tissues (transmissive methods)
- methods where the boundaries of the organs are detected (reflective methods)
- methods where the subject receives a dose of radioactive tracer material which tends to accumulate in a specific organ. The transversal scintigraph is then formed on the basis of the radiation emitted by that organ (emissive methods).

Transmissive methods: Roentgen transversal tomography, an old and well known process, is the most common of the transmissive methods. The procedure currently in use has been developed by Watson[2]. The subject rotates continuously around its central axis. The motion of the film cassette is synchronized to that rotation, both axes being parallel. The radiation coming through the subject reaches the film at an angle. (The angle between the ray beam and the rotation axis of the patient varies from 65 to 75 degrees.) Since the rotations are synchronized, all points in the plane to be radiographed remain in a stationary position relative to the film, while radiation striking the film from points outside that plane moves in circular paths and is thus mixed into a diffused background. Takahashi and Matsuda[3] have developed a transversal tomograph where the subject is radiographed in a prone position.

Farmer and Collins[4] have recently described a transversal tomograph which uses ^{137}Cs as a radiation source. A tightly collimated monoenergetic (662 keV) beam of gamma radiation is scanned through the subject at various levels in the transversal plane (Fig. 1). The Compton radiation scattered from the area under examination is detected laterally. The wave

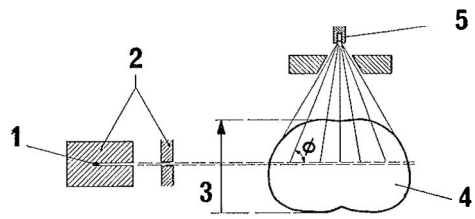

Fig. 1. Transversal tomography method of Farmer and Collins[1] 1. ^{137}Cs radiation source 2. Collimators 3. Scanning motion of the source 4. Patient 5. Radiation detector.

length λ (and the energy) of the Compton quanta varies according to the scattering angle ϕ as follows:

(1) $\Delta\lambda = k(1 - \cos\phi)$

where $\Delta\lambda$ = change in wave length
k = Compton wave length of an electron (0.024 Å)
ϕ = angle of scattering.

Thus in the energy spectrum measured by a multichannel analyser, a given energy corresponds to a definite position. The intensity of that energy is a function of the electron density of the scattering element as well as of the density of the interjacent material. The energy spectra of all scanned positions are combined in a computer and corrected for subject absorption of the primary and scattered radiation and for the angular intensity distribution of the scattered radiation given by the Klein-Nishina equation. The result is an outline and a density distribution of the transversal area examined.

Hounsfield[5] has suggested a procedure where the subject would be irradiated from various directions, and the transmitted radiation would be registered by a scintillation counter. In his proposal, an oscillatory motion of the source would replace the linear scan, and the subject would rotate within the area swept by the radiation beam. The results could be recorded on magnetic tape for computer manipulation. No practical adaptation of the procedure are given.

Reflective methods: Ultrasonic waves are reflected from tissue surfaces. If a receiver crystal is mounted together with the transmitter crystal, the depth of these surfaces can be calculated from the times required by the echoes to return to the receiver crystal. A cross-sectional view is obtained by moving the probe along the skin of the subject. The positional coordinates of the probe and the time delays of the echoes, converted to distances, are represented on the screen of an oscilloscope tube. Obviously, this method can also furnish a sectional view of any plane swept by the beam of ultrasonic waves, and is thus not limited to a transversal plane.

Emissive methods: Emissive transversal radiography consists in measuring the radiation emitted by an area in a subject to construct a cross-sectional view of that area. The patient receives prior to the taking of the radiograph a radionuclide which specifically accumulates in the organ under study. Thus these methods belong to the radioisotope scintigraphic methods.

Two different procedures of emissive gamma tomography have been developed. Kuhl and Edwards[6] have based their method on the use of the

scintiscanner. Their arrangement consists of two scintillation counters mounted in axial opposition and whose fields of view have been collimated into a common narrow beam. The subject lies between these detectors. The detector pair moves laterally and registers the transversal distribution of the subject radioactivity. The detectors rotate 7.5° around the subject, another scan is made and a new radioactivity distribution is registered. This process is continued until the detectors have made one complete rotation in equal increments of 7.5°. The distribution obtained at the various angles are finally combined by a digital computer to construct a transversal tomogram.

Anger *et al.*[7] in their procedure use a gamma camera (Anger camera) having a large detector crystal of approximately 30 cm in diameter. This allows the entire transverse distribution of the gamma radiation at each angular position to be registered at one time, since the camera measures both the intensity of the radiation and its spatial distribution (position sensitive detector). As the subject rotates around its central axis, a transverse distribution is obtained from every direction. Anger built the final picture from these distributions using an oscilloscope. Each distribution is represented on the screen by a column of dots: a heavy concentration of isotope results in a large number of dots. This pattern is photographed through a Maddox lens, which spreads each dot into a line perpendicular to the direction of the dot column. The camera rotates around the axis of the oscilloscope tube, and its angular speed is synchronized to the angular motion of the subject. As the shutter remains open during one full revolution of the camera, an image is integrated on the film to form a cross-section of the subject radioactivity.

2. The purpose of the present investigation

The purpose of this work is to present a new transversal tomographic process using a radionuclide as a source of gamma radiation and a scintillation counter as a radiation detector. This process is termed Transversal Transmission Gammatomography (TTGT):

- *transversal*, since the radiograph obtained is a cross-section of the subject;
- *transmission*, since the radiograph is constructed from radiation transmitted through the subject;
- *gamma*, since the radiation source is a gamma-emitting radionuclide;
- *tomography*, since the radiograph is the representation of a single plane.

The present work shall first consider the equipment and components required and the image constructing mechanism. Then the properties of

the tomograms obtained and the effect of the different components on these properties shall be discussed. Finally, some considerations on the constructional aspects of a prototype shall be given.

3. Equipment and image formation in transversal transmission gammatomography

This presentation of transversal transmission gammatomography begins with a general description of the necessary equipment and of the interrelations between the various components. A schematic explanation of the image construction process is given.

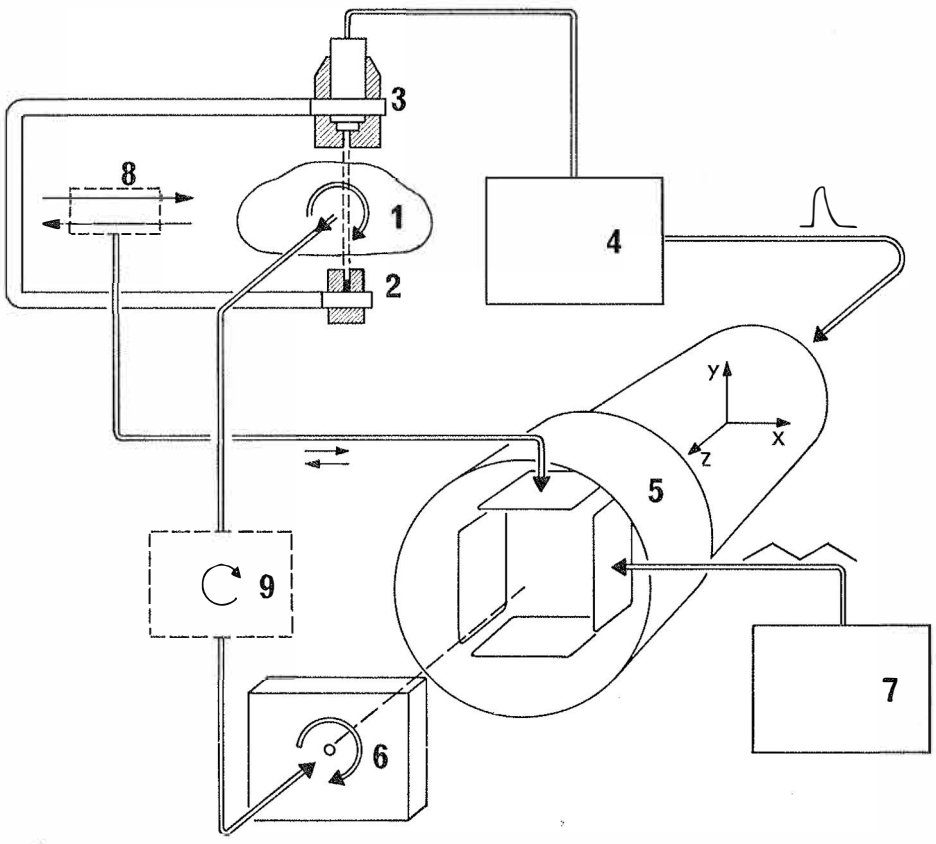

Fig. 2. Schematic representation of TTGT equipment 1. Patient 2. Radiation source 3. Radiation detector 4. Pulse height analyser 5. Oscilloscope 6. Oscilloscope camera 7. Pulse generator 8. Scan mechanism and coordinate transfer system 9. Rotation mechanism.

3.1. TTGT equipment

The components required are schematically illustrated in Fig. 2. These include the following units:

1. The patient or object of which a cross-sectional radiograph is desired.
2. A shielded radiation source whose radiation field is limited by a straight collimator to a narrow beam.
3. A radiation detector whose field of view is collimated to match the emission beam of the source.
4. A pulse height analyser for the radiation detector. This unit gives a standard sized and shaped output pulse for each pulse »accepted» by the energy channel.
5. An oscilloscope whose electron gun is triggered for the duration of the output pulse of the pulse height analyser.
6. A motorized oscilloscope camera which rotates around the central axis of the cathode ray tube.
7. A pulse generator which can furnish either a sawtooth or triangular waveform.
8. A transverse mechanism to scan the emitter-detector unit (2, 3) at a constant speed across the subject. The unit includes a position coordinate transfer system to the oscilloscope.
9. A rotation mechanism to synchronously rotate the subject (1) and the oscilloscope camera (6).

3.2. Interconnections and relative motions of TTGT components

The radiation emitter (2) and the radiation detector (3) are rigidly mounted opposite each other so that the radiation beam falls within the field of view of the detector. In other words, the units are mounted in coaxial opposition. The emitter-detector unit is given an even transversal motion, so that the beam scans across the subject (1). A potentiometer is linked to this traverse so that its output voltage varies linearly with the position of the emitter-detector pair (0 being at mid-travel). This tension is fed to the Y deflecting plate of the cathode ray tube (CRT): thus a given position of the emitter-detector pair results in a given vertical position of the electron beam on the CRT screen. As the measurement point moves from one edge of the object to the other, the trace on the CRT screen is correspondingly displaced along the Y axis.

The pulses from the radiation detector go to the pulse height analyser (4), which lets only those falling within the energy channel move onwards to the **Z** axis of the oscilloscope (5). These pulses trigger the CRT beam for a definite length of time. Thus every pulse having a given energy level generates a flash of light on the oscilloscope screen. The vertical position

of that light dot is determined by the transversal position of the emitter-detector pair at that instant.

The pulse generator (7) feeds a triangle voltage to the X deflecting plate of the CRT. The amplitude of that waveform is selected so that the trace is shifted horizontally across the entire face of the screen. If the frequency of the triangle waveform is low relative to the duration of the triggered electron streams, the pulses show up as small dots spread horizontally across the face of the tube. However, if the triangular waveform has a high enough frequency, the traces are stretched into horizontal lines on the screen. A frequency of 10 to 100 kHz is used in practical tomography.

After the emitter-detector unit has completed one scan, a motor rotates the base on which the subject stands to a new angular position relative to the radiation beam, and a new scan is initiated. The angular motion of the oscilloscope camera photographing the screen is synchronized to the rotation of the subject. The camera rotates around the central axis of the oscilloscope tube. The angular motion of the subject and of the camera is in equal increments of approximately 10° for at least half a revolution or a whole multiple thereof. The motion of both units can also be continuous.

3.3. Tomogram construction

The construction of a TTGT image is shown in Figs. 3 and 4. The radiographed subject is a cylindrical object made up of concentric layers of

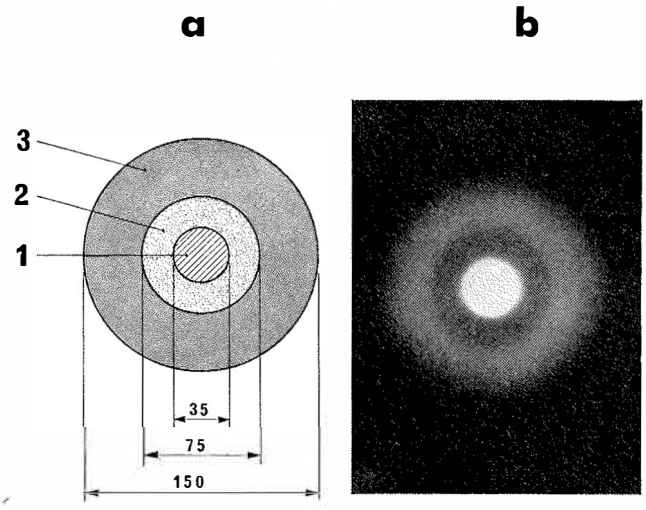

Fig. 3. a) Circular base cylindrical phantom 1. Aluminum cylinder (ϱ = 2.7 g/cm^3) 2. Balsa layer (ϱ = 0.15 g/cm^3) 3. Water layer. Dimensions are in millimeters
b) Roentgen transversal tomogram of this cylinder.

differing densities (Fig. 3 a). The materials used are water (1), balsa wood (2) and aluminum (3). These correspond, in an exaggerated fashion to the tissue densities of muscles, lungs and bones. The radiography plane is perpendicular to the cylinder axis. Fig. 3 b shows a roentgen transversal tomogram of that phantom.

As the emitter-detector pair moves from one edge of the object to the opposite, the pulse rate registered at any one time depends on the amount of material interposed between the source and the detector. This is expressed by the gamma radiation attenuation law (Fig. 4 a):

$$I(x) = I_0 e^{-\sum_{i=1}^{3} \mu_i d_i(x)} \tag{2}$$

where $I(x)$ = detected intensity at coordinate x
I_0 = intensity incident on the subject
μ_i = linear attenuation coefficient $\{i = 1, 2, 3$ (water, balsa, Al)$\}$
$d_i(x)$ = material thickness at coordinate x.

As the CRT screen is continuously photographed during a traverse, a column of dots is formed on the film, the dots being spread according to

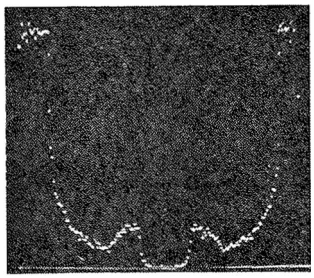

a

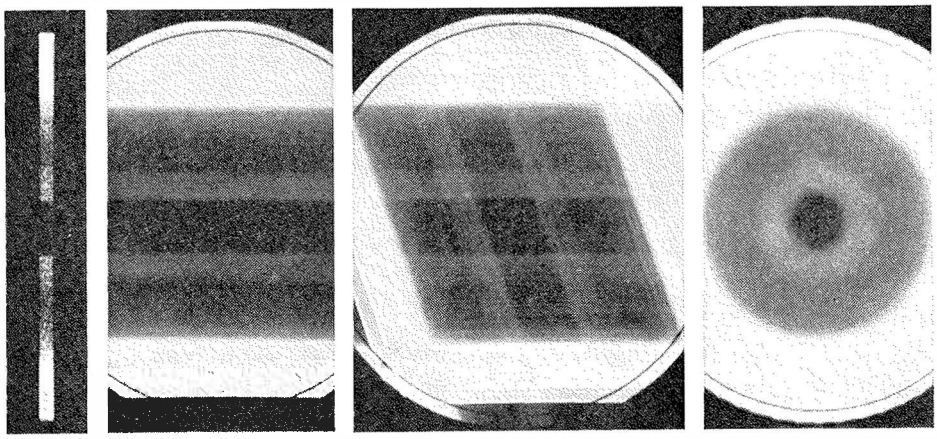

b c d e

Fig. 4. Image construction in the TTGT process
a) Intensity profile of the transmitted radiation
b) Dot column corresponding to the intensity profile
c) Belt pattern resulting from the spreading of the dot column by a triangular waveform of pulse generator
d) Two intersecting belt patterns
e) Final image

equation (2) (Fig. 4 b). Connecting the output voltage of the pulse generator to the X deflecting plate of the CRT spreads each dot of the column as a line across the entire screen. The result is shown in Fig. 4 c, where the areas of differing radiation attenuation are brought out as horizontal belts. Once the belt pattern of one traverse has been registered on the film, the subject and the oscilloscope camera are rotated through a definite angle, and a new traverse is initiated. The pattern of belts generated at each angular position is superposed on the preceeding ones as the camera shutter is kept open. Fig. 4 d shows two superposed belt patterns. The set of superposed belt patterns obtained after a complete angular revolution of the subject forms the final transversal transmission gammatomographic image (Fig. 4 e).

The image of a single point of the object on the film is the sum of the radiation intensities reaching the detector from the set of angular positions. This is expressed by the equation

$$(3) \qquad I(x\,,\,y) = \sum_{j=1}^{n} I_0 e^{-\sum_{i=1}^{3} \mu_i d_i(x,\,y;\,\phi_j)}$$

where $I(x\,,\,y)$ = intensity registered belonging to coordinates x, y
n — number of equidistant angular positions
I_0 = intensity incident on subject
μ_i = linear attenuation coefficient (see equation 2)
$d_i(x\,,\,y\,;\,\phi_j)$ = thicknesses of layers at coordinates x, y measured along direction ϕ_j.

Equation (3) shows that a tomogram can be constructed though the subject and the oscilloscope camera are kept in a continuous rotary motion as long as a sufficiently large number of angular positions ϕ_j are generated for each point (x, y). This is achieved by having a rapid transversal motion relative to the angular motion. The phantom images used in this work have all been made using continuous rotary motion.

4. TTGT process components

This chapter presents the components required by the TTGT process. The technical and physical properties which fundamentally affect the imaging procedure or the graphical properties of the process are also discussed.

4.1. Radiation source

One of the most important parameters affecting the quality of a TTGT image is the source of radiation. In selecting a source, the following characteristics should be noted:

— the gamma-ray energy of the source
— the gamma-ray yield of the source
— the half-life of the radionuclide, and
— the availability and price of the source.

The first two of these factors will be considered on the basis of practical calculations in order to be able to define the optimum radiation source. Although this paper limits itself to gamma radiation, other types of radiation, such as Bremsstrahlung, might be applicable to this process.

4.11 Gamma-ray energy of radiation source

The influence of gamma-ray energy on the radiographic imaging procedure is defined on the basis of the radiation attenuation law of narrow-beam geometry:

$$(4) \qquad I(E) = I_0 e^{-\mu(E)x} .$$

The parameters studied are the intensity $I(E)$ of the radiation emerging from the subject, the relative changes in intensity $\Delta I(E)/I(E)$ as the attenuation properties of the interposed material vary and the corresponding changes in statistical information measured as the number of standard deviations $\Delta I(E)/\sqrt{I(E)}$. This last parameter could be termed »statistical contrast». All these parameters will be treated as functions of gamma-ray energy (E).

Practical calculations are based on a body of water 20 cm thick (the approximate thickness of a patient). The changes ΔI in the intensity of the radiation emerging from the subject are examined by replacing a 1.0 cm thick layer of water with 1) a 1.0 cm thick layer of lung tissue (water mass

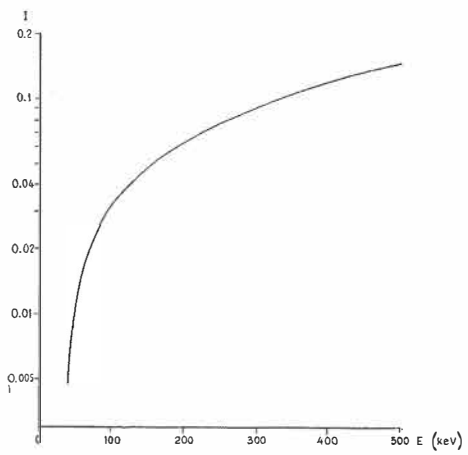

Fig. 5. Intensity I of the emerging radiation as a function of energy E ($I_0 = 1$, water layer 20 cm thick).

attenuation factor, density $\varrho = 0.25$ g/cm³) and 2) a 1.0 cm thick layer of bone tissue ($\varrho = 1.9$ g/cm³). The mass attenuation factors are taken from the White-Grodstein tables[8], some of the values for various energies having been interpolated from the table values.

The results are diagrammed in Figs. 5, 6 and 7. Fig. 5 shows that the radiation transmitted through the subject rises approximately 8 times as the gamma energy increases from 50 to 300 keV. On the other hand, Fig. 6 indicates that the relative change in transmitted radiation (contrast) for the same increase in energy is reduced to about 0.5 of the original values by a 1 cm layer of lung, and correspondingly to about 0.25 by a 1 cm layer of bone. These opposite trends are partly compensated in the case of the »statistical contrast» (Fig. 7). The curve has a maximum at 60 keV for the variations through the bone layer, while the curve for the lung layer slopes upwards continuously, although slowly. At higher energy levels (over 100 keV), very little change occurs in the »statistical contrast». For the 1.0 cm layer of bone tissue, the constant value is 24 % lower than the maximum value.

So far this seems to indicate that the most favourable energy level would be 60 keV. At that level, the contrast ($\Delta I/I$) and the »statistical contrast» ($\Delta I/\sqrt{I}$) values are advantageous. However, this requires a source having a high gamma-ray yield to obtain an emerging intensity sufficiently large for the imaging process. As far as the statistical information is concerned, higher energy levels are roughly as favourable as the optimum level. When the image is formed on film, both contrast and »statistical contrast» are important for picture quality. If the data is manipulated

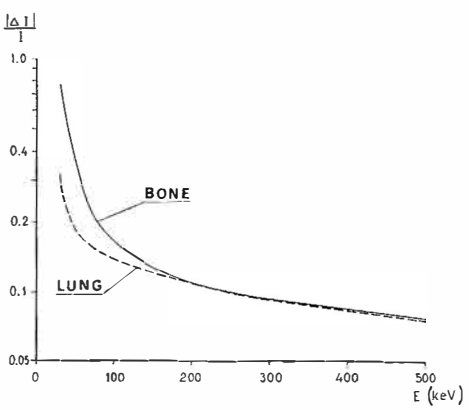

Fig. 6. Relative change $|\Delta I/I|$ of emerging radiation as a function of energy E when a 1 cm layer of water is replaced with corresponding thicknesses of bone and lung.

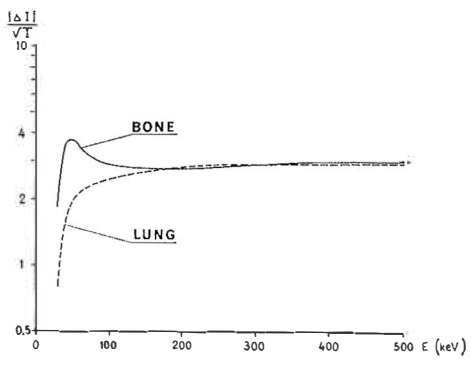

Fig. 7. Variation of »statistical contrast» $|\Delta I/\sqrt{I}|$ as a function of energy E for a situation similar to Fig. 6 ($I_0 = 10000$ counts)

quantitatively, statistical information becomes paramount. In that case contrast can be increased by removing a constant portion of background.

The curves indicate that gamma energies lower than 50 keV are useless for transversal transmission gammatomography.

The above discussion applies to a one-dimensional imaging process. However, since the final tomogram is a summation of the pulses obtained at differing angular positions, the results can be generalized to encompass an entire TTGT.

The radiation energy employed also puts constraints on the collimation and shielding of the source and affects the efficiency of detection. The quantitative discussion of these subjects are not entered into. However some remarks on their qualitative aspects are in order:

- the heavy shielding demanded by high gamma-ray energy sources makes the construction of the apparatus more difficult
- energetic gamma-ray radiation penetrates through the collimator walls at a higher rate than low energy radiation, and image sharpness suffers
- the detection efficiency of the NaI (Tl) crystal is lower for high energy gamma radiation. Thus high energies require thicker crystals.

4.12 Gamma yield of radiation source

To obtain a reasonably short radiographic exposure and to ensure that a statistically significant number of pulses are registered on the tomographic image, the gamma yield of the source must be sufficiently high. On the other hand, a sharp picture demands a source as small as possible. An appraisal of the gamma yield of any source must take into account the following factors:

- the activity and specific activity of the source
- its mode of disintegration (number of principal gamma quanta per disintegration)
- its geometry and self-absorption.

The TTGT process is based on the narrow-beam geometry. Thus a cylindrically shaped source would be suitable. The self-absorption factor B for a source of that shape is given by the equation

$$B = \frac{1 - e^{-\mu l}}{\mu l} \tag{5}$$

where μ = linear attenuation coefficient of the source
l = cylinder length.

When the emitter and the detector are collimated as a coaxial unit, the number N of gamma particles per unit time reaching the detector is

$$(6) \qquad N = A \cdot f \cdot \frac{a}{4\pi r^2} \cdot B$$

where A = source activity
f = number of principal gamma quanta per disintegration
a = area of detector collimator opening
r = emitter-detector distance
B = self-absorption factor.

Geometrical resolution (sharpness) requires that the detector collimator limits the radiation beam diameter to less than 5 mm. A picture needs at least 100000 pulses to avoid excessive statistical fluctuation, and the exposure time must be less than 10 minutes. These boundary values will be used in discussing the sources used in this investigation.

4.13 Radiation sources used in this work

Americium-241: ^{241}Am has a half-life of 458 years and a principal gamma-ray energy of 60 keV. The source has an activity of 100 mCi and is manufactured by Radiochemical Centre, Amersham, England (Code: AMC 6). The encapsulated source is shown in Fig. 8.

Equation (5) gives a self-absorption value of 0.20 when

μ = 72.5 1/cm
l = 0.07 cm.

The number of gamma quanta reaching the detector per unit time is given by equation (6) as 400 c/s, when the following values are used:

A = 100 mCi $\times$ 3.7 $\times$ 10^7 c/s · mCi
f = 0.36
a = 0.20 cm^2
r = 49 cm
B = 0.20.

It should be noted that this calculation considers only the radiation of the Am source passing through the collimator opening (3.5 mm ⌀).

Assuming that the patient has an elliptical cross-sectional shape where the lengths of the major and minor axes are 35 and 20 cm respectively a 60 keV gamma radiation would have to penetrate an average thickness of about 15 cm in the TTGT process. Adding to this the boundary conditions listed at the end of section 4.12, it is concluded that gammatomography requires a ^{241}Am source having an activity of approximately 450 mCi.

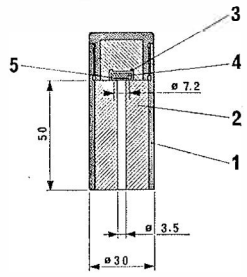

Fig. 8. Shielded ^{241}Am source 1. Brass shell 2. Lead wall 3. Steel shell 4. Tungsten alloy backing 5. ^{241}Am-source Dimensions are in millimeters.

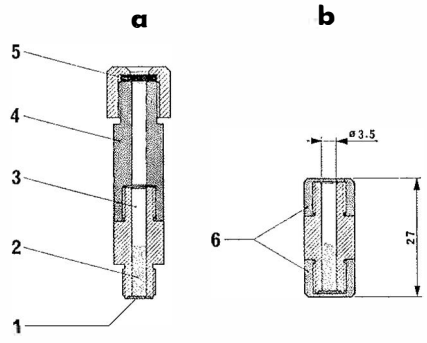

Fig. 9. Manufacture of ^{99m}Tc source
a) Source and solution container
b) Encapsulated source 1. Metal gauze through which solution is dripped out 2. Ion exchange resin where ^{99m}Tc is retained 3. Liquid reservoir 4. Percolator tube 5. Rubber plate through which ^{99m}Tc solution is injected into the reservoir 6. Cover.

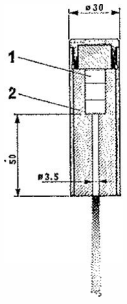

Fig. 10. Shielded ^{99m}Tc source and a photograph of the emission field. 1. Source 2. Lead shield

Technetium-99m: ^{99m}Tc has a half-life of 6 hours and a gamma-ray energy of 140 keV. The source used in the TTGT was made by a method similar to the one suggested by Sorenson *et al.*[9]. A pertechnetate solution (activity 20 to 200 mCi/20 ml) is eluted with NaCl saline and the solution is percolated through the ion exchanger resin column (Dovex 1×8, 100/200 mesh), where the pertechnetate is retained by the resin (Fig. 9). The retention percentage after two successive runs varies from 95 to 100. This resin column is then used as the source. Fig. 10 shows the encapsulated column and a photography of the radiation field.

From equation (5), a self-absorption factor of 0.90 is obtained for a technetium source, when

$\mu = 0.19$ 1/cm
$l = 1.0$ cm.

The number of gamma quanta reaching the detector per unit time, as determined from equation (6), is 220 c/s · mCi when the following values are used:

$A = 3.7 \times 10^7$ c/s · mCi
$f = 1.0$
$a = 0.20$ cm^2
$r = 49.5$ cm
$B = 0.90$.

The minimum activity for an utilisable technetium source is about 8 mCi.

4.2. Detector and collimators

4.21 Detector

The detector used in this gammatomographic process is the scintillation counter forming part of a Picker isotope scanner (Picker Magnascanner III). The crystal is a cylindrical NaI (Tl) crystal 2″ thick and 3″ in diameter. At the gamma-ray energies employed, the gamma quanta absorption in the crystal is 100 %. The aluminum window on the crystal does not bring about any noticeable attenuation of the entering radiation.

4.22 Collimators

For gammatomography, a set of single hole collimators were fabricated. The collimators were made of lead, except for the shell and the threaded section. Both rectangular and circular collimators were used. The rectangular collimator openings were 15 mm high, and 1.5, 3.0 and 5.0 mm wide. The circular collimator openings had diameters of 1.5 and 3.0 mm. The depths of the collimators were 8 cm.

The radiation penetrating through the shell and the collimator wall does not noticeably widen the field of measurement. At 140 keV the half-value distance of gamma radiation in lead is 0.3 mm.

4.3. Emitter-detector unit

The emitter and the detector are supported as a unit on an U-shaped arm (Fig. 11). The radiation field of the emitter and the opening of the collimator are adjusted coaxially opposite each other. The distance between the throat of the U and the radiation beam is 40 cm. The distance between the source and the detector can be set anywhere between 31 and 53 cm, which means that the free space between the collimators varies from 18 to 40 cm. The emitter mounting allows the orientation of the radiation beam to be altered

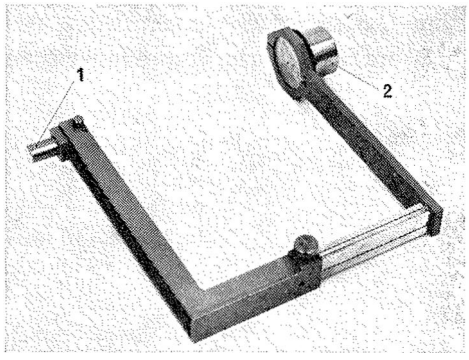

Fig. 11. Emitter-detector unit 1. Radiation source 2. Collimator

if necessary. The entire unit is screwed to the scintillation counter using the collimator threads.

4.31 Unit traverse mechanism and transmission of positional coordinates to oscilloscope

The emitter-detector unit is traversed by the detector head motor of the Picker scanner. Maximum travel is 36 cm, and the speed is steplessly adjustable between 8 and 200 cm/min. The motor powers the arm through a rack and pinion.

A gear mounted on the shaft of a Helipot potentiometer and meshed to the motor drive gear forms the transversal coordinates transfer system. A definite position of the arm corresponds to a definite position of the potentiometer slide contact. Equal voltages of opposite sign are fed to each end terminal of the potentiometer. The tension at the slide contact is led to one of the Y deflecting plates of the oscilloscope, the opposite plate being at ground potential. A full deflection of the oscilloscope electron beam requires an input tension of $\pm$ 2 V. The tension at the potentiometer terminals can be varied from $\pm$ 2 V to $\pm$ 6 V. At the lower tension, the full travel of the arm results in the full deflection of the electron beam. At $\pm$ 6 V, a traverse of $\frac{1}{3} \times 36 = 12$ cm is enlarged to fill the entire oscilloscope screen.

The potentiometer voltage source has a stability better than 0.5 % and a ripple inferior to 0.1 %. The stability of the traverse positional coordinates transfer system is such that no shift in the position of the light spot on the CRT screen can be detected for a fixed position of the arm. The zero tension point, which also corresponds to the center of subject rotation, remains in position during the tomogram construction period to within 0.5 mm.

4.4. Pulse transfer from detector to oscilloscope

Pulses are transmitted from the scintillation counter to the CRT through the pulse height analyser of the Picker scanner. The output pulse of the analyser is led to the unblank input of the oscilloscope to trigger the electron gun. The oscilloscope employed is the CRT section of a gamma camera (PhoGamma III, Nuclear Chicago) used in standard gamma scintigraphy. The screen has a diameter of 9 cm. The channel level of the pulse height analyser was adjusted at 50 keV and the channel width at 20 keV using ^{241}Am; the corresponding values were 130 keV and 20 keV respectively for a ^{99m}Tc source. The system has an energy resolution of 20 % for ^{241}Am and 12.5 % for ^{99m}Tc, when the photomultiplier high tension is set at 950 V. This setting does not give optimal energy resolution, but has the advantage that the energy channel adjusting scales correspond directly to the radiation energy levels expressed in keV.

The unblank pulse to the oscilloscope has an amplitude of 30 V and it lasts 23 μs. This pulse triggers the CRT electron gun and a light spot is visible on the screen for the same length of time. The light spot intensity is adjustable through a ten turn potentiometer furnished with a scale.

4.5. Pulse generator

The pulse generator used is a Wavetek Voltage Controlled Generator Model III. Its output is a triangular waveform of 2 V amplitude and having a direct current component of 0 *V*. This means that the zero level was situated on the central axis of the screen and that the waveform peaks corresponded to a full deflection across the screen ($\pm$ 4.5 cm). The linearity of the waveform was checked by photographing it on the CRT screen. As no measurable deviations were detected, linearity was held to be sufficient for TTGT imaging purposes.

When constructing the final image from single points, a frequency of 30 Hz was used. For tomographic images built up from single lines, the frequency was raised to 30 kHz. One electron beam burst was thus spread on the CRT screen to a length of 13 cm.

This triangular waveform was fed to one of the X deflecting plates of the tube, the opposite plate being at ground potential.

4.6. Rotation of subject and image forming plane

The subject stands on a base rotated by a synchromotor at an angular speed of 0.25 rpm. A scale is attached to the base so that a tomogram could be formed from a series of static images taken at equidistant angular positions. The rotation of the image plane is achieved by making the

Polaroid camera photographing the CRT screen rotate around the CRT axis. The camera is mounted on a bearing surrounding the CRT screen and is driven by a synchromotor geared to that bearing.

The play in both motion is so small that it is not noticeable on the image, nor was any shift of the axes of rotation detectable from the image.

4.7. Photographing the CRT screen

The image on the oscilloscope screen was photographed using a Polaroid oscilloscope camera and Polaroid photographic paper Polapan 107 (speed 3200 ASA, resolution 22—28 lines/mm). The images to be densitometrically measured were taken on Polaroid transparent film 46-L (speed 800 ASA, resolution 32—35 lines/mm).

4.8. Practical TTGT procedure

The initial step consists in centering the axes of the various motions.

First, the zero level of the coordinate transfer potentiometer must be matched to the central position of the emitter-detector pair. The pair being at midtravel, the sliding contact of the potentiometer is brought exactly to the center of the resistor, and then the voltage applied to the potentiometer is regulated to bring the zero level to that contact point. This procedure simultaneously brings the light spot to the middle of the Y axis on the CRT screen. This alignment is verified by photographing with the camera held at differing angular positions the line pattern created by the emitter-detector pair at its central position. An exact adjustment results in all the lines crossing at one point. This adjustment remains stable for many weeks to within approximately 0.3 mm on the CRT screen.

Next the rotation axis of the base is adjusted to cross the emitter-detector beam (which is still centered). To perform this a thin metallic bar is used as an absorber. The bar is mounted vertically to coincide with the rotation axis of the base. The base is then displaced to bring the bar within the beam and finely adjusted for maximum attenuation, i.e. until the detected intensity is minimum. This signifies that the axis of the beam passes through the center of the bar, and therefore the mid-traverse position and the base axis are coincident. This adjustment can be carried out to within 0.5 mm.

To construct a tomogram, the subject should stand as symmetrically as possible over the axis of the base, as this centers the image on the film. The emitter-detector unit is then adjusted vertically to the level to be radiographed. Then a single pass is made and the total number of pulses detected is registered. This value is used to set the intensity of the CRT

electron beam according to normal gamma camera practice. An estimate of the photographic time is also made.

The rotary speed of the subject in the present tomographic procedure was held constant at one revolution in four minutes. The traverse speed varies from 100 to 200 cm/min, which provides 10 to 20 different angular positions for each rotation. Since the rotary period (T) is not an entire multiple of the traverse time (t_0), i.e.

$$T \neq n \cdot t_0 \tag{7}$$

the angular positions relative to the detector head are spread evenly over many rotations, and no influence of this continuous rotation is discernible from the photography. The exposure times vary from 4 to 16 minutes for $^{99\,m}$Tc and 30 to 40 minutes for ^{241}Am.

5. Imaging in transversal transmission gammatomography

In this chapter, various phantom images are qualitatively examined. A quantitative analysis develops the modulation transfer functions (MTF) for the separate components and for the complete system. The general properties of the imaging process are also discussed on the basis of MTF measurements.

5.1. Phantom images

5.11 Images of anatomical phantom

Images of an anatomical phantom were constructed using the Alderson phantom[10], where layers of mass having the same densities as normal tissues are cast on natural bones. The mass densities were checked with the gamma-ray absorption method using ^{241}Am nuclide as a radiation source. The density of the mass corresponding to the lungs was measured as 0.4 g/cm^3 and that of the remaining soft tissues as 0.94 g/cm^3. The bone densities were 1.8 g/cm^3 in the cranial region and 1.1 g/cm^3 in the pelvic area. These measured values differ markedly from the values for live tissue. Woodard[11] gives the density of the compact cortical bone (fresh wet weight) as varying from 1.79 to 1.93 g/cm^3 (average 1.87 g/cm^3). Dahl and Vikterlöf[12] provide a value of 0.16 g/cm^3 for lung tissue. Figs. 12 and 13 show tomographic images of the lung area (Alderson phantom plate 18). Fig. 12 a is a standard X-ray radiograph taken in a direction perpendicular to the plate surface. Fig. 12 b is a roentgen tomogram of the same plate. Figs. 13 a and 13 b are TTGT images of this plate made with ^{241}Am and $^{99\,m}$Tc respectively.

The roentgen tomogram is clearly more detailed than the TTGT images. On the other hand the TTGT images present a better contrast between the

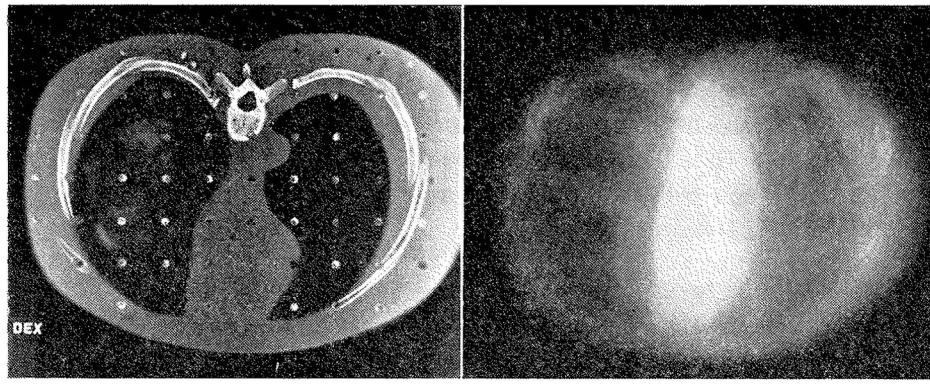

a b

Fig. 12. Alderson phantom plate 18 (lung region)
a) Roentgen image
b) Roentgen transversal tomogram

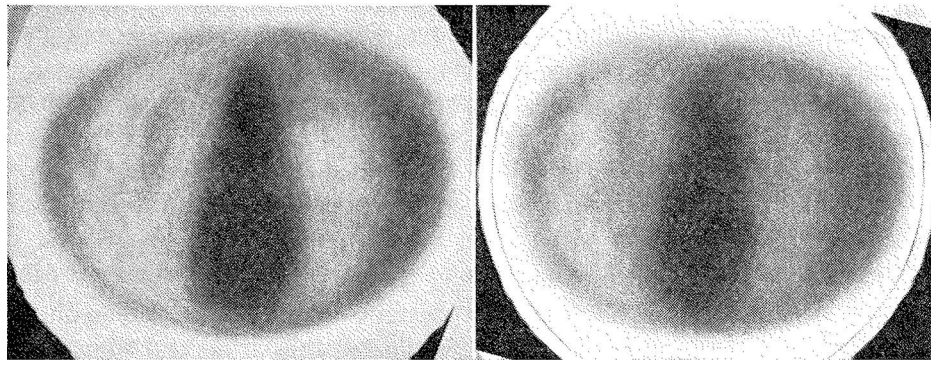

a b

Fig. 13. TTGT image of lung region
a) ^{241}Am source used
b) ^{99m}Tc source used

lung tissues and the remaining tissues. The thickening in the right lung area (Fig. 13 a) is somewhat discernible on the TTGT images, but is not evident on the roentgen tomograms. A peculiarity of the tomograms is that when moving from the external region to the internal, a convex boundary surface stands out clearly. However, if that surface contains a concave depression, that area becomes almost undiscernible. This is detectable at the spinal depression and where the left lung forms wedges towards the central axis. The phenomenon can be qualitatively explained in that the intensity of the radiation passing through such a depression is strongly

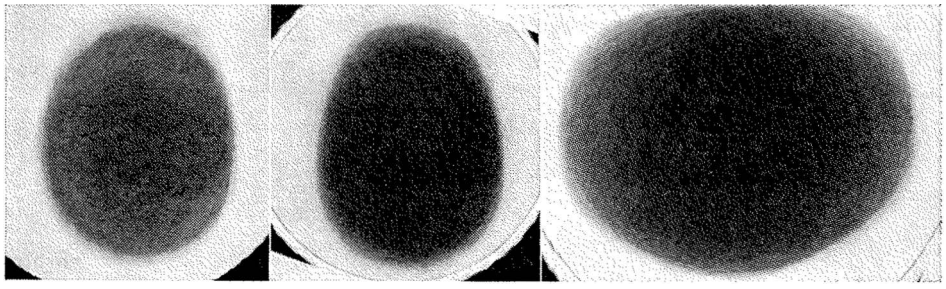

a b

Fig. 14. TTGT image of cranial region (Alderson phantom plate 4)
a) ^{241}Am source used
b) ^{99m}Tc source used

Fig. 15. TTGT image of pelvic region (Alderson phantom plate 28) made with ^{99m}Tc source

affected by the attenuative properties of the medium behind the boundary surface.

There are no remarkable differences between the tomograms made with Americium and those made with Technetium, except that the lower pulse rate of the former source results in more obvious statistical unevenness.

Fig. 14 shows Americium and Technetium tomograms of the cranial region (Alderson phantom plate 4). The cranial bone boundary stands out most clearly on the ^{241}Am tomogram. Fig. 15 shows a ^{99m}Tc tomogram of the Alderson pelvic phantom (plate 28). The osseous structure is not distinct, due most probably to the low density of the phantom bones relative to the remaining mass.

5.12 Images of water phantom

The phantom is a straight plexiglass cylinder of elliptical cross-section. Its major and minor axes are 26 and 20 cm long respectively. The cylinder is filled with water, and to provide some details it contains an aluminum tube of 3.5 cm diameter and 0.5 cm wall thickness, and an aluminum cylinder of 3.5 cm diameter surrounded by a balsa shell 2.0 cm thick. These cylinders are lined on the major axis of the ellipse.

Fig. 16 shows a sketch of the phantom (a), a transversal roentgen tomogram (b) and a TTGT (c) made with ^{99m}Tc of the same phantom Tomograms have also been made with ^{241}Am. Densitometric measurements of the tomograms were made along lines A and B of Fig. 16 a. The results are diagrammed on Fig. 17. Although the curves show the greater sharpness obtainable through roentgen tomography, the TTGT images present a greater contrast $\Delta I/I$ between the various details. For instance $|\Delta I/I|$

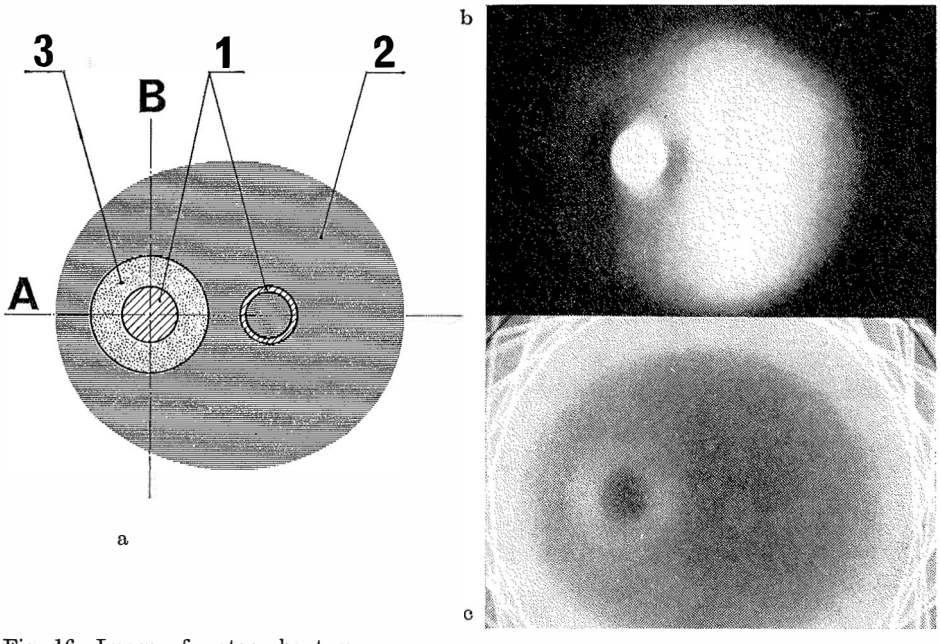

Fig. 16. Image of water phantom
a) Diagram of phantom 1. Aluminum 2. Balsa 3. Water
b) Roentgen transversal tomogram
c) TTGT image made with ^{99m}Tc source

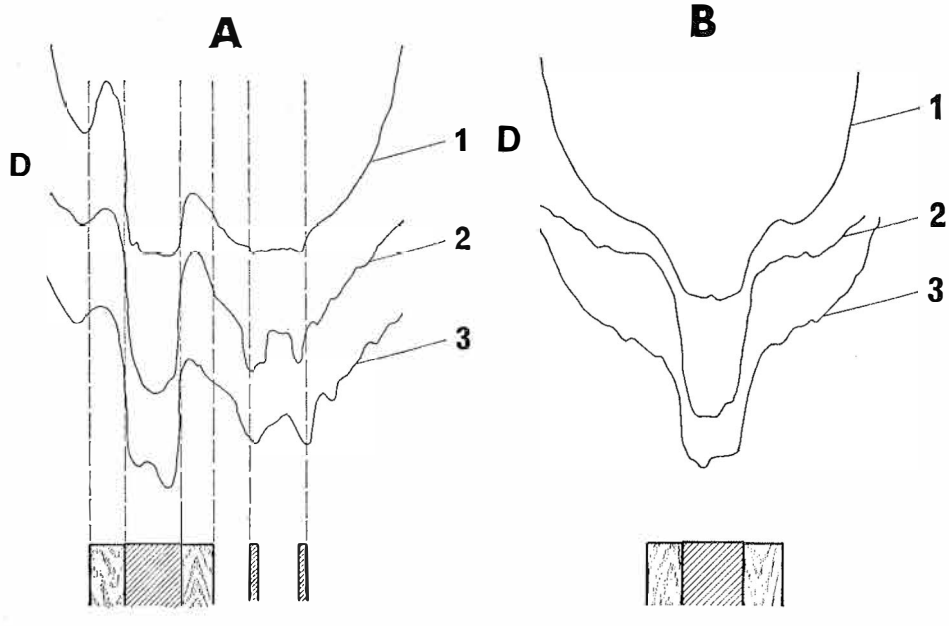

Fig. 17. Photometric curves along directions A and B (Fig. 16 a) 1. Roentgen 2. ^{241}Am TTGT 3. ^{99m}Tc TTGT
The density (D) scale is arbitrary but identical for the three curves

in the region of the aluminum tube has values of 0.1(roentgen), 0.4 (^{241}Am) and 0.4 (^{99m}Tc). Also there is a clear anisotropic pattern in the images along the perpendicular axes A and B. The contrast due to the balsa layer is low along direction B. The statistical fluctuation is more pronounced in TTGT images.

5.13 Image of a patient

Fig. 18 shows a gamma tomogram of the thoracic region of a healthy patient. The lungs and the heart shadow are clearly visible. All boundary lines are very diffuse. The principal reason for this is that the rotary table used for phantom radiography had been made without any supports or harness for the patient, who obviously moved during the exposure. The exposure lasted four minutes using a 100 mCi ^{99m}Tc radioisotope as radiation source. The detector had been fitted with a circular collimator of 3 mm in diameter.

5.2. Modulation transfer function of the TTGT components and system

The modulation transfer function (MTF) is commonly used to express the image transmission properties of optical systems[13]. It is also used to quantitatively measure the entire image forming system and the reproduction fidelity of single components in roentgen radiography[14] and radioisotope scanning[15] process. In the TTGT process, the modulation transfer functions of the emitter-detector pair and of the recording system are initially presented, and then the modulation transfer function of the entire system is developed.

The starting point in imaging transfer theory is the transfer of a Dirac δ-function from the object space to the image space through the imaging system. This transfer can be written using an operator (H) to represent the system. The δ-function

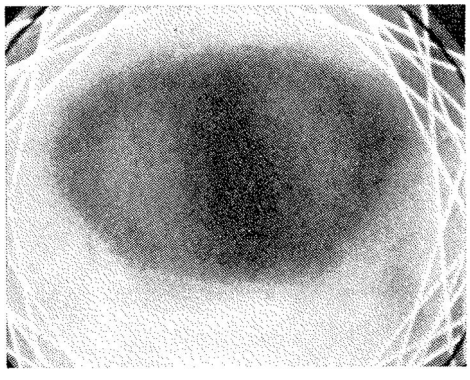

Fig. 18. Patient image of lung region made with ^{99m}Tc

(8) $\delta(x - \xi , y - \eta)$

is transformed into a representation of an image

(9) $H\{\delta (x - \xi , y - \eta)\} = h(x - \xi , y - \eta)$

This image is called the point spread function $\{\mathrm{PSF}(x, y)\}$. An object can be represented as an integral of δ-function:

$$(10) \quad f(x , y) = \int_{-\infty}^{+\infty}\int f(\xi , \eta)\ \delta(x - \xi , y - \eta)\ d\xi d\eta$$

where $f(\xi, \eta)$ is a numerical weighting factor. Using the operator H, the image $g(x, y)$ of that object becomes assuming that the transform is linear:

$$(11) \quad g(x , y) = H\{f(x , y)\} = \int_{-\infty}^{+\infty}\int f(\xi , \eta)\ H\{\delta(x - \xi , y - \eta)\}\ d\xi d\eta$$

or

$$(12) \quad g(x , y) = \int_{-\infty}^{+\infty}\int f(\xi , \eta)\ h(x - \xi , y - \eta)\ d\xi d\eta\ .$$

A Fourier transformation of this convolution integral gives it the form:

(13) $G(u , v) = F(u , v)\ H(u , v)$

where

$$(14) \quad G(u , v) = \int_{-\infty}^{+\infty}\int g(x , y)\ e^{-2\pi i(ux - vy)}\ dx\ dy$$

F and H have similar forms. $H(u, v)$ is the modulation transfer function $\{\mathrm{MTF}(u, v)\}$ of this system. It gives the transformation from the Fourier transform in the object space to the Fourier transform in the image space.

The equation (14) is still valid when the object is represented by a single δ-function. Since the Fourier transform of the δ-function is a constant, the modulation transfer function can be calculated from the point spread function according to the equation:

$$(15) \quad \mathrm{MTF}(u , v) = F(u , v) = \frac{\int_{-\infty}^{+\infty}\int \mathrm{PSF}(x , y) \cos 2\,\pi(ux + vy)\ dx\ dy}{\int_{-\infty}^{+\infty}\int \mathrm{PSF}(x , y)\ dx\ dy}$$

where MTF(u, v) is normalized to unity at zero spatial frequency. The Fourier transform of the PSF includes only the real part (Fourier cosine transform), since the radiation used is incoherent

In experimental work, the one-dimensional line spread function (LSF) is used. The MTF is then calculated from the equation

$$\text{(16)} \quad \text{MTF}(\nu) = \frac{\int_{-\infty}^{+\infty} \text{LSF}(x) \cos 2\pi\nu x \, dx}{\int_{-\infty}^{+\infty} \text{LSF}(x) \, dx} .$$

If the transforms brought to the images by each imaging component are linear, the modulation transfer function for the entire system, $\text{MTF}_{\text{tot}}(\nu)$, is the product of the MTF of the individual components or

$$\text{(17)} \quad \text{MTF}_{\text{tot}}(\nu) = \prod_{i=1}^{n} \text{MTF}_i(\nu) .$$

5.21 Modulation transfer function of the emitter-detector unit

The principal component of a TTGT apparatus is the emitter-detector unit, and obviously it has a fundamental influence on the accuracy of the imaging. The standard method to measure the modulation transfer function of an image forming system consists in using a narrow slit as the object; this corresponds to the Dirac δ-function in the object space. In such a case the line spread function is determined directly from the image of the slit.

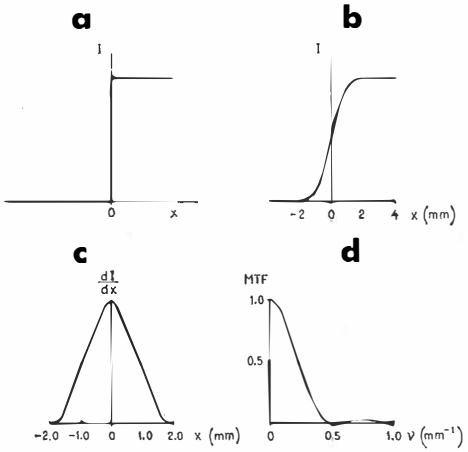

Fig. 19. Diagrammatic representation of the determination of the modulation transfer function from a step function
a) Step function
b) Image of the step function (3 mm opening)
c) Derivative of the image (line spread function)
d) MTF (ν = spatial frequency) calculated after the equation (16)

The modulation transfer function of the emitter-detector unit has been determined as follows: the object is a lead wall opaque to the radiation energy employed. As the emitter-detector unit moves past the edge of that wall, and the detector begins to register radiation, the step function $S(x)$ is imaged as an S-shaped curve. The Dirac δ-function is the formal derivative of the step function, i.e $\delta(x) = dS(x)/dx$, and similarly in the image space, the image of the δ-function (the line spread function), is the derivative of the edge image. The MTF is calculated from this line spread function. The MTF is determined diagrammatically in Fig. 19.

Fig. 20 shows the MTFs for the 1.5 and 3.0 mm circular collimator openings. The measurements have been made using both ^{241}Am and ^{99m}Tc. The MTF curves do not bring out any noticeable differences between the two radionuclides (Fig. 20 a), or between measurements made in air or through a 20 cm thick water layer (Fig. 20 b). The similarity of the curves proves that, at the energy values employed in this work, the penetration of the collimator remains low and that scattered radiation does not noticeably degrade the image.

5.22 Modulation transfer function of the recording unit

The MTF of the recording complex (pulse height analyser, oscilloscope, pulse generator, and photography), forming a continuation of the emitter-detector unit, was obtained using a method whereby the input to the system was a Dirac δ-function and so the output was a line spread function. The object to be imaged was the radiation beam of the stationary emitter-detector unit, the resulting image a line on the oscilloscope screen. This

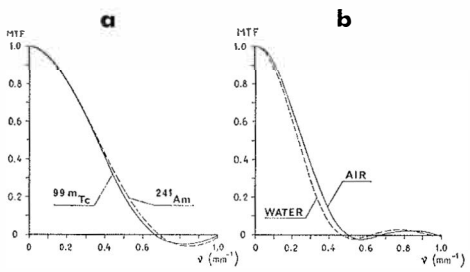

Fig. 20. Modulation transfer functions of the emitter-detector unit
a) 1.5 mm opening measured in air
b) 3.0 mm opening measured with ^{99m}Tc

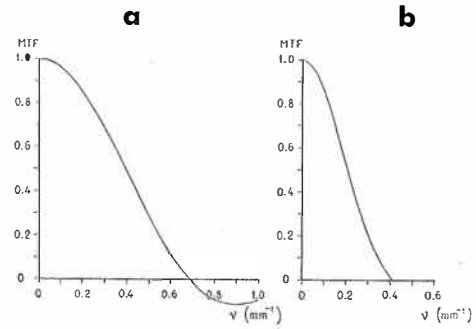

Fig. 21. a) Modulation transfer function of recording system
b) Total modulation transfer function of emitter-detector unit (3.0 mm opening) and of the recording system {MTF (Fig. 20 b) × MTF (Fig. 21 a)}

line was photographed on Polaroid 46-L transparent film, and its LSF determined using a densitometer (Adam Hilger H 451) having a slit opening of 0.2 mm. The MTF corresponding to such a slit opening is approximately unity in the spatial frequency region of TTGT image formation, and therefore it has no distorting effect on the result.

The MTF of the recording system is shown in Fig. 21 a, and the total MTF of a TTGT process traverse in Fig. 21 b. The latter is the product of the modulation transfer functions of the emitter-detector unit and of the recording system (equation (17)). This multiplication is allowable, since the components are linear, the output of the emitter-detector unit is measured directly in pulses, the recording system operates in the linear portion of the sensitivity curve of the film emulsion and density units are used in the densitometric measurements.

The MTF of the recording system is of the same order of magnitude as that of the emitter-detector unit. Therefore the recording system — in this case obviously the oscilloscope — definitely degrades the TTGT image. This is quantitatively apparent from the product MTF curve in Fig. 21 b.

5.23 Effect of rotary motion on modulation transfer function

In the TTGT process, the image of each point is constructed according to equation (3). Lines on the CRT screen corresponding to various orientations intersect at the point under consideration and are summed on the film in the oscilloscope camera. In a similar fashion the image of a point object, the point spread function, is the sum of the line spread functions in various orientations. The point spread function profile thus formed in a certain direction is therefore the sum of the projections of the different line spread functions on that direction (ϕ_0):

$$\text{PSF}_{\phi_0}(x) = \frac{1}{n} \sum_{i=0}^{n} \text{LSF}_{\phi_i}(x) \tag{18}$$

where

$$\text{LSF}_{\phi_i}(x) = \text{LSF}_{\phi_0}(x \cos |\phi_i - \phi_0|) \,. \tag{19}$$

Fig. 22 a shows a point spread function formed from equations (18) and (19) starting from the line spread function of the recording system. The modulation transfer function for the recording system and the rotary motion in Fig. 22 b was obtained from the PSF of Fig. 22 a. Fig. 22 b also shows the same MTF calculated directly from the densitometrically measured point (Fig. 23 a), which is an intersection of multidirectional lines.

The point spread function of Fig. 23 a is symmetrical, since it corresponds to the axis of a circular cylinder and the attenuation expressions

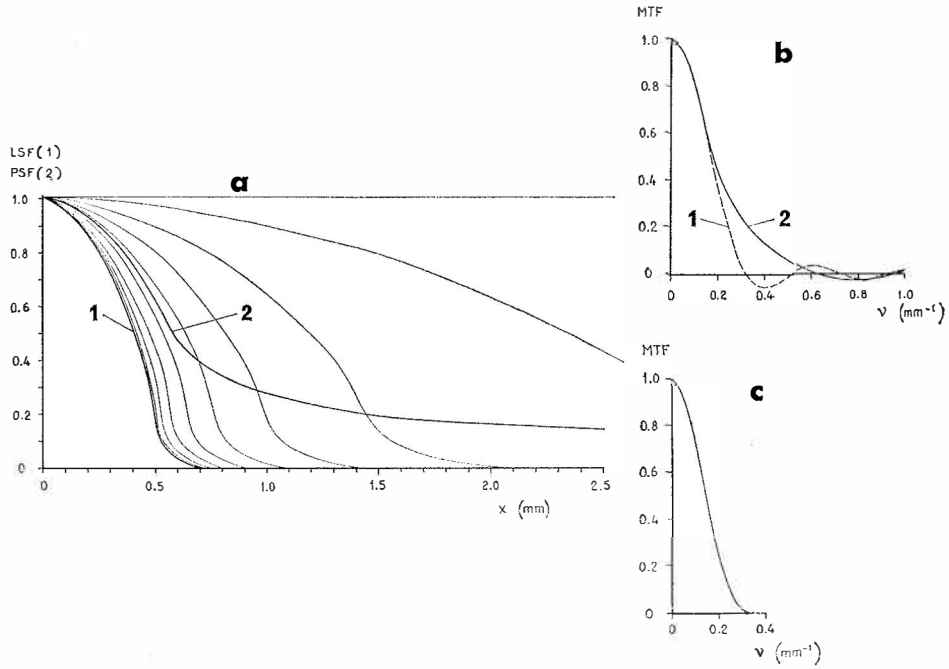

Fig. 22. a) Generation of point spread function (2) from the line spread function (1) according to equations (18) and (19). (The thin lines are projections of the LSF on directions differing by increments of 10°)
b) Modulation transfer function of the rotary motion 1. Determined from a photometric measurement of a point in an image (Fig. 23a) 2. Determined from the point spread function of Fig. 22 a
c) Modulation transfer function of entire system at the center of the cylinder {MTF (Fig. 20 b) × MTF (Fig. 22 b 1)}

(20) $I_0 e^{-\mu x(\phi_i)}$

for the various orientations ϕ_i are equally large.

If this symmetric attenuation does not exist, and it usually does not, a weighting function for the attenuation in the ϕ_i direction must be added to the LSF term of that direction. Thus the point spread function and at the same time the MTF are dependent upon the entire system to be imaged. Fig. 23 b shows a tomogram of a point in an asymmetrical attenuation environment.

5.24 Modulation transfer function of the entire system

The modulation transfer function of the rotary motion is not a function representative of the imaging system. In fact, it varies with the object

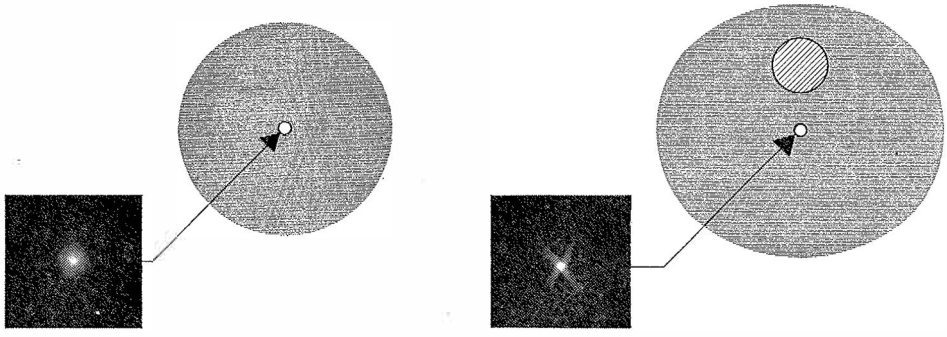

a b

Fig. 23. Point image in the TTGT process
a) Center of a circular base cylinder
b) Point in an asymmetrical surrounding

to be imaged. Therefore equation (17) cannot be used to calculate the MTF representing the entire imaging system. However, in Fig. 22 c this has been done formally for comparative purposes in order to obtain the MTF of an entire system, although only in the exceptional case of a circular cylinder.

Modulation transfer functions are used to describe the imaging properties of a system. They can also be used to improve an image by starting from the Fourier transform of that image, and working backwards through the MTF of the system to obtain the Fourier transform of the subject. An inverse transform will then furnish a »copy» of that subject. A loss of information occurs after those values of the spatial frequency where the MTF reaches zero. In TTGT, modulation transfer functions do not lend themselves to such constructive ends, but can only be employed to compare the process to other imaging methods.

5.3. General properties of the TTGT image

One can deduce already from the imaging procedure that the constructed image is conformal to the cross-section of the subject.

If the radiographed area includes a convex boundary between two regions of unequal densities (Fig. 24 a), obviously the points P_1 and P_2 on either sides of the boundary are imaged with differing intensities. When the points are sufficiently close to each other, the radiation attenuation in the angles α is identical. However, in the angles β the attenuation expressions differ, corresponding to the density differences.

Should area 1 include a concave boundary (Fig. 24 b), these conclusions are no longer valid. Both points on either side of the boundary may have

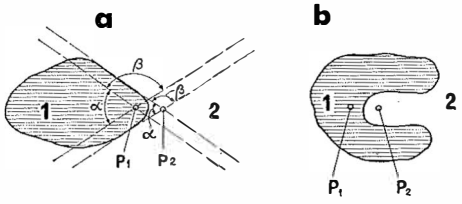

Fig. 24. Imaging of points on either sides of boundary surfaces
a) Convex area
b) Point near concave area

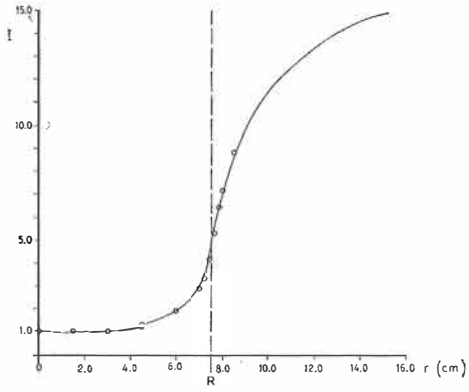

Fig. 25. Homogeneity of the TTGT image of a straight cylinder of radius R ^{99m}Tc as source. A value of 1.0 has been given to the intensity I at the axis of the cylinder

similar attenuation conditions making the intensity differences undiscernible in the TTGT image. Therefore the image of a given point depends on the attenuative properties of the surroundings. This same phenomenon appeared earlier when discussing the modulation transfer function of the rotary motion. As mentioned, this expression varied as a function of the position of the point and furthermore was dependent upon the shape and density differences of the subject. The imaging is therefore *non-isoplanatic*. In a narrower sense this non-isoplanatic property appears as *anisotropy* and the point spread function is asymmetric (Fig. 23 b).

The *inhomogeneity* of the image is most easily detected when radiographing a subject of constant density. Fig. 25 illustrates such a case. The intensity profile of the image of a water filled circular cylinder has been calculated from equation (3) at angular increments of 10°. The curve also includes experimentally measured values, which were obtained by rotating the subject around an axis passing through the point under examination. The number of pulses detected during one complete revolution of the subject was registered with the emitter-detector unit remaining stationary. Besides inhomogeneity within the subject, the image intensity rises as the distance increases outside the subject boundary.

6. Radiation doses in the TTGT process

As the TTGT process makes use of radiation, the doses given to the subject must be estimated. This chapter presents the calculations of the upper limits of the skin and integral doses for both ^{241}Am and ^{99m}Tc.

To determine the skin exposure dose, the dosage equation of a point source is used:

$$(21) \qquad D_0 = \Gamma \cdot \frac{B \cdot A \cdot t}{r^2}$$

where D_0 = skin exposure dose

Γ = dose constant $\left(\text{for Am: 0.3 and for Tc: 0.7 } \frac{\text{R} \cdot \text{cm}^2}{\text{h} \cdot \text{mCi}}\right)$

B = self-absorption factor (for Am: 0.20 and for Tc: 0.90)

A = source activity (for Am: 450 mCi and for Tc: 8 mCi)

t = irradiation time of skin area

r = source-skin distance (10 cm).

In the TTGT process a new area is continuously being irradiated and the irradiation period is spread over the subject circumference as follows:

$$(22) \qquad t = \frac{d}{s} \cdot T$$

where d = width of radiation field on skin (0.5 cm)

s = circumference of subject (80 cm)

T = image construction time (10 min).

From these values, which are approximated towards the maximum dosage, the following upper limits for skin exposure doses are obtained:

$D_0(\text{Am}) < 0.3$ mR, and
$D_0(\text{Tc}) < 0.06$ mR.

The integral dose is calculated from the following equation[16]:

$$(23) \qquad \Sigma = \frac{D \cdot T \cdot a}{\mu}$$

Σ = integral dose

D = dose rate on the skin

a = area of irradiated field on the skin (0.5 cm^2)

μ = linear attenuation coefficient of tissue (for Am: 0.19 cm^{-1} and for Tc: 0.16 cm^{-1}).

This expression gives the upper limit of the integral dose, since it assumes a subject thickness large enough to completely absorb the radiation. The dose rate $D(= D_0/t)$ is obtained from equation (21), noting that rad $\simeq R$. The following upper limits of integral dose are obtained

$\Sigma(\text{Am}) < 0.15\ g \cdot \text{rad}$
$\Sigma(\text{Tc}) < 0.04\ g \cdot \text{rad}$

The skin exposure doses of roentgen tomography are of the order of 2.0 R[17]; the TTGT process doses are thus less than 0.02 % of the roentgen tomography doses. The radiation doses of conventional scintigraphic procedures are also some orders of magnitude greater than those of the TTGT process.

7. Discussion

7.1. General conclusions

The present study shows the possibility of constructing an apparatus to make transversal tomograms using a gamma emitting radionuclide as the radiation source and a scintillation counter as the detector. The process results in an image sharpness superior to standard radioisotopic scintigraphy, although inferior to roentgen methods (Fig. 26). The 5 percent threshold values[19] in MTF are 0.04 mm^{-1} for scintigraphy 0.35 mm^{-1} for TTGT and 2.5 mm^{-1} for roentgenography. The radiation doses in the TTGT process are minimal: less than 0.02 % of the doses used in transversal roentgentomography.

There were no detectable differences in the results between the sources with different gamma-ray energies: ^{241}Am (60 keV) and ^{99m}Tc (140 keV). However it might prove difficult to obtain a sufficiently active ^{241}Am source. A ^{99m}Tc source, on the other hand, is easily made in the isotope laboratory from the commonly used ^{99m}Tc pertechnetate solution.

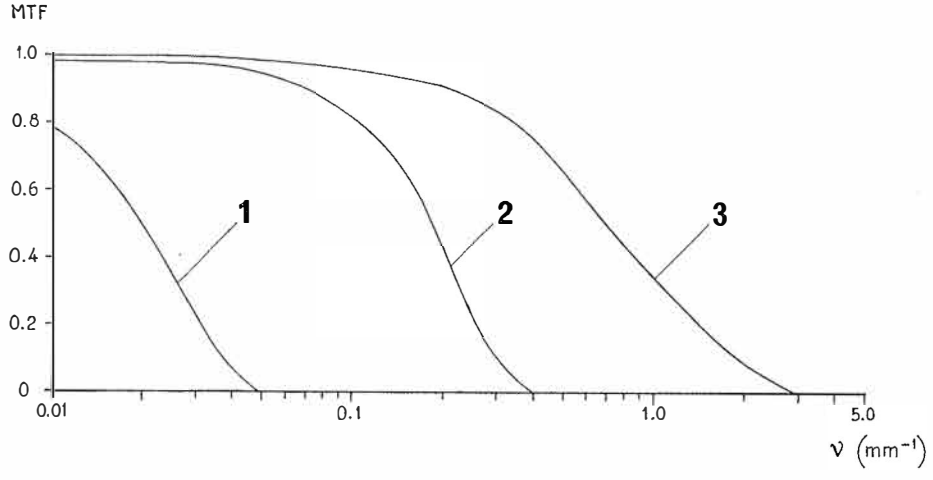

Fig. 26. Comparison of modulation transfer functions of different imaging processes
1. Radioisotope scintigraphy[15] 2. TTGT process 3. Roentgenography (film and screen »Diamant»)[18]

The exposure times employed in this work lasted 4—40 minutes. Increasing the diameter of the collimator opening up to 7 mm should reduce the exposures to one or two minutes with ^{99m}Tc as a source.

Since the TTGT process involves rotary motion, ordinary transfer theories cannot be used to describe quantitatively the image properties. On the other hand, as the primary information is acquired in digital mode, it should be feasible to present the results in a quantitative form through computer manipulation.

Image fidelity in the TTGT process is sufficient for treatment planning in radiotherapy. As it is possible to build a TTGT apparatus to radiograph a prone patient and since the use of ^{99m}Tc allows the pelvic region to be radiographed, it is obvious that transversal transmission gammatomography greatly widens the scope of tomography in radiotherapy. The breathing motion degrades the image sharpness of the thoracic region, but that motion is present during the radiation treatment as well. The profile measurement obtained from a traverse can be used quantitatively with the method of Holt and Laughlin[20] to calculate the tissue corrections of the doses. A quantified output of the TTGT process could also be utilized for computer treatment planning in radiotherapy.

7.2. Comparison with roentgen transversal tomography

References to roentgen tomography have been made in many instances in this work. A summary is given here of the main differences between the gamma and roentgen tomographic processes:

— the TTGT process results in an image of inferior sharpness (Fig. 26)
— the TTGT images seem to have superior contrast (Figs. 12, 13, 17)
— the radiation doses in TTGT method are smaller
— the statistical fluctuation is more pronounced in the TTGT images
— a TTGT apparatus is easily built to radiograph a prone patient
— tomograms of the pelvic region are possible.

The classical explanation of the formation of a roentgen tomographic image is as follows[21]: the radiation penetrates the patient at an angle and projects the cross-section of the patient on the film plane. Due to the synchronized motion the points external to the plane of radiography are blended into a diffuse background. Yet the technical procedure of roentgen transversal tomography is quite similar to the TTGT process. The transversal motion of TTGT is replaced in roentgen tomography by a radiation cone enclosing the entire area under examination. The summation of the profile images from various directions is arrived at through rotary motion. Thus the attenuation differences which lead to the formation of a TTGT image also explain the operation of roentgen transversal tomography. One

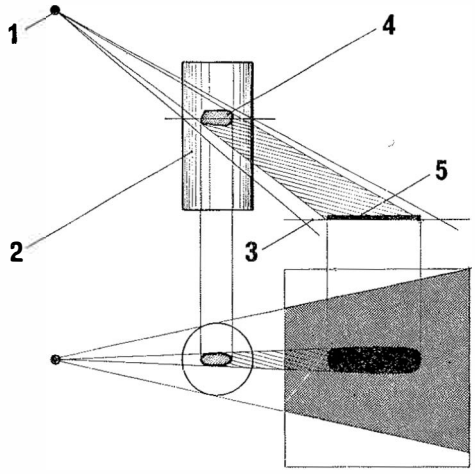

Fig. 27. Roentgen transversal tomography
1. Roentgen tube 2. Object to be imaged 3. Film 4. Detail in imaged plane 5. »Shadow» of detail

dissimilarity between these methods, however, can be illustrated through a situation in roentgen tomography where a detail on the plane to be imaged extends only partly across the cone in the axial direction of the subject (Fig. 27). The attenuated belt is then limited to the corresponding area of the film, and it does not disturb the remainder of the picture. On the other hand, if the detail is situated outside of the image plane but still within the radiation cone, it makes a shadow on the film and is thus an extra source of noise in roentgen transversal image. Therefore the TTGT process is a special case of roentgen transversal tomography in that the direction of projection is within the plane to be imaged (zero projection angle), and the spreading of the image on the film is performed electronically.

7.3. Design aspects

Many constructional changes must be made to the equipment when planning for patient radiography on the basis of the apparatus used in this work, which has been designed only for phantom radiography.

The collimator opening of the emitter-detector unit can be increased in size from the 3 mm diameter mainly used in this work up to 5 or even 7 mm, which would result in speed increases of 2.8 to 5.4 times. The scintillation counter can be small, a suitable thickness, and diameter, would be 1.5 cm. Because of the radioisotopes employed, the collimator walls can be made of lighter metal such as brass lead only as an inner lining. This would result in a construction of lesser weight and the motion mechanisms would become easier to design. Adding rotary motion to the emitter-detector unit means that the subject is stationary and therefore could also be lying

down. A suitable traverse length, and at the same time distance between emitter and detector, seems to be 50 cm; the angular speed of the rotary motion would be one to two revolutions per minute.

The sharpness of the image obtained at the oscilloscope screen has an important influence on the sharpness of the final image, so that a careful choice must be made for the final equipment. The rotation of the screen image was solved here by rotating the camera, although obviously the picture could be rotated electronically using between X and Y plates in CRT sine wave modulation synchronized with emitter-detector unit rotation.

The effect of the photographic emulsion on the image was not considered in this work. It might prove possible through the use of other emulsions than Polaroid to obtain a finer gradation in the final picture.

In general, a transversal transmission gammatomograph can be built using simple mechanical construction and the measuring system also is composed of standard electronic and radiation measuring components.

Acknowledgements: I wish to express my deep gratitude to Professor Erik Spring, who followed the progress of my work and gave valuable advice and help.

I am also indebted to Professor Juhani Kantele for his help and critical comments.

The completion of my work would not have been possible without the many-faceted help given by Valmet Oy. Particularly I am indebted to Mr. T. Honkavaara and to Mr. Antti Lehtinen.

To Dr. Eeva Nordman I wish to express my gratitude for the excellent working facilities and her interest in my work. To Mr. Hannu Olkkonen I am indebted for his help in the measurements and calculations.

Mr. André H. Faure translated the manuscript into English and Mrs. Terhi Räsänen did the typing. I express my thanks to both for their skilful work.

When starting this work I received financial support from the Emil Aaltonen Foundation, which is hereby gratefully acknowledged.

Jyväskylä, April 1972

AHTI REKONEN

References

1. G. MUEHLLEHNER, Phys. Med. Biol. 16 (1971) 87.
2. W. WATSON, USA patent 283720 (1939).
3. S. TAKAHASHI and T. MATSUDA, Radiology 74 (1960) 71.
4. F. T. FARMER and M. P. COLLINS, Phys. Med. Biol. 16 (1971) 577.
5. G. N. HOUNSFIELD, Bundesrepublik Deutschland, Deutsches Patentamt. Offenlegungsschrift 1941433 (1970).
6. D. E. KUHL and R. Q. EDWARDS, Radiology 83 (1964) 926.
7. H. O. ANGER, D. C. PRICE and P. E. YOST, J. Nucl. Med. 8 (1967) 314.
8. G. WHITE-GRODSTEIN, Natl. Bur. Std. (U.S.) 583 (1957).
9. J. A. SORENSON, R. C. BRIGGS and J. R. CAMERON, J. Nucl. Med. 10 (1969) 252.

10. S. W. ALDERSON, L. H. LANZL, M. ROLLINS and J. SPIRA, Am. J. Roentgenol. 87 (1962) 185.
11. H. G. WOODARD, Health Phys. 8 (1962) 513.
12. O. DAHL and K. J. VIKTERLÖF, Acta Radiol. Suppl. 189 (1960) p. 40.
13. K. ROSENHAUER and K.-J. ROSENBRUCH, Rep. Progr. Phys. 30 (1967) 1.
14. K. ROSSMANN, Radiology 93 (1969) 257.
15. J. H. CHRISTIE and W. J. MACINTYRE, Medical Radioisotope Scintigraphy, Proceedings of a Symposium, Salzburg, 6.—15. August, 1968. International Atomic Energy Agency, Vienna 1969, p. 457.
16. H. E. JOHNS, The Physics of Radiology, Charles C. Thomas, Springfield, Second Edition (1966) p. 356.
17. L. ZAZULA, Belastung des Patienten bei diagnostischen Röntgenuntersuchungen (Durchleuchtungen und Aufnahmen). Diss. Erlangen 1949.
18. O. DÜNISCH, M. PFEILER and H. KUHN, Electromedica 39 (1971) 114.
19. O. SCHOTT, Die Modulations Übertragungsfunktion in der Röntgenologie in F.-E. Stieve (Hrsgb): Bildgüte in der Radiologie. Gustav Fischer Verlag Stuttgart 1966, p. 76.
20. J. G. HOLT and J. S. LAUGHLIN, Radiology 93 (1969) 161.
21. A. GEBAUER and F. WACHSMAN, Röntgenblätter 2 (1949) 215.

Contents

Societas Scientiarum Fennica
Communicated March 21, 1972 by E. Spring and L. Simons
Printed May 1972
Keskuskirjapaino—Centraltryckeriet
Helsinki—Helsingfors